

Supplementary Materials for

Linkage-specific deubiquitylation by OTUD5 defines an embryonic pathway intolerant to genomic variation

David B. Beck, Mohammed A. Basar, Anthony J. Asmar, Joyce J. Thompson, Hirotugu Oda, Daniela T. Uehara, Ken Saida, Sander Pajusalu, Inga Talvik, Precilla D'Souza, Joann Bodurtha, Weiyi Mu, Kristin W. Barañano, Noriko Miyake, Raymond Wang, Marlies Kempers, Tomoko Tamada, Yutaka Nishimura, Satoshi Okada, Tomoki Kosho, Ryan Dale, Apratim Mitra, Ellen Macnamara, Undiagnosed Diseases Network, Naomichi Matsumoto, Johji Inazawa, Magdalena Walkiewicz, Katrin Öunap, Cynthia J. Tiff, Ivona Aksentijevich, Daniel L. Kastner, Pedro P. Rocha, Achim Werner*

*Corresponding author. Email: achim.werner@nih.gov

Published 20 January 2021, *Sci. Adv.* 7, eabe2116 (2021)
DOI: 10.1126/sciadv.abe2116

The PDF file includes:

Figs. S1 to S10
Legends for tables S1 to S5
List of members of the Undiagnosed Diseases Network (alphabetical order)

Other Supplementary Material for this manuscript includes the following:

(available at advances.sciencemag.org/cgi/content/full/7/4/eabe2116/DC1)

Tables S1 to S5

Supplemental Materials

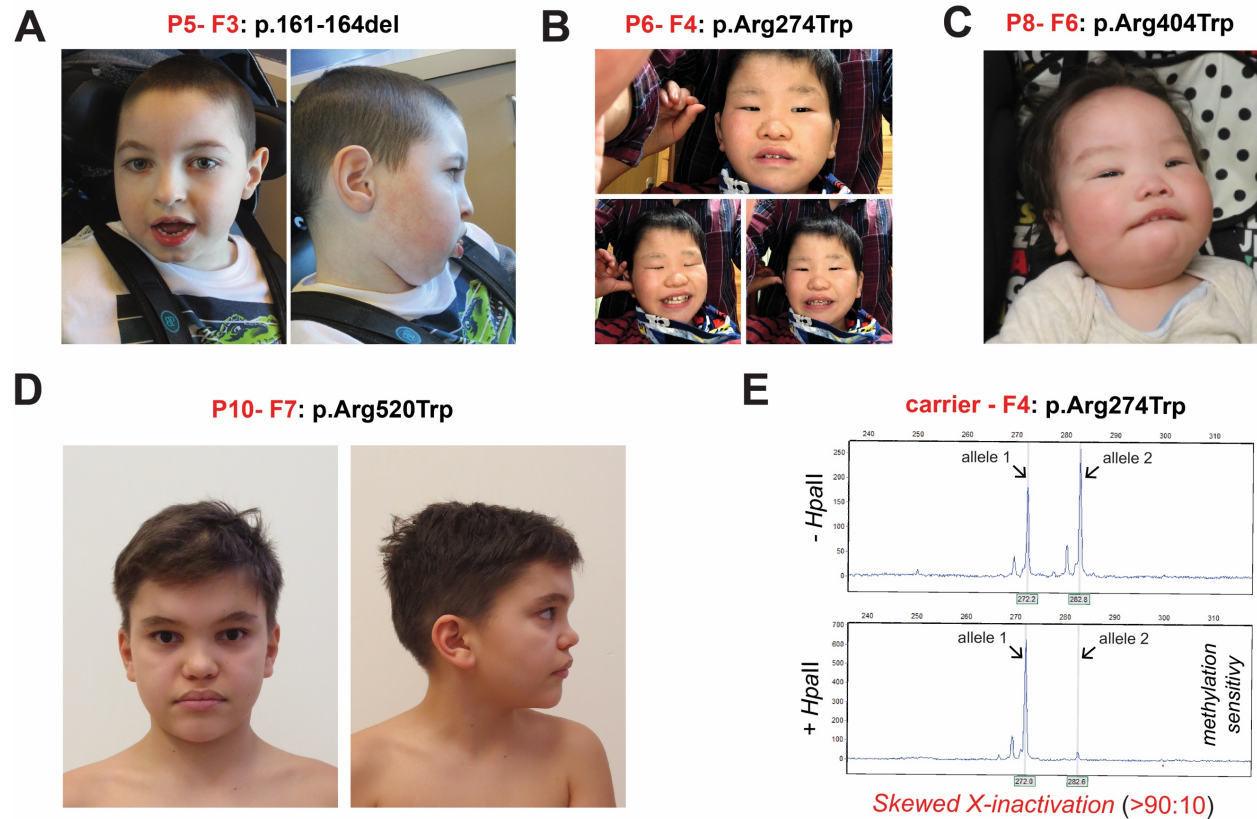


Fig. S1: Additional OTUD5 patient photos and skewed X-inactivation in OTUD5 carrier-F4

A. Clinical photos of patient P5-F3 carrying the p.161-164del mutation. **B.** Clinical photos of patient P6-F4 carrying the p.Arg274Trp mutation. **C.** Clinical photos of patient P8-F6 carrying the p.Arg404Trp mutation. **D.** Clinical photos of patient P10-F7 carrying the p.Arg520Trp mutation. **E.** The *OTUD5* p.Arg274Trp carrier mother exhibits skewed X-inactivation, as revealed by digestion of genomic DNA with a the methylation-sensitive restriction enzyme *HpaII* followed by PCR amplification of the human androgen receptor (*AR*) gene at Xq12 and capillary gel electrophoresis. DNA was isolated from peripheral blood. Photo credit for A-D: With permission of the subjects' legal guardian.

^{FLAGHA}OTUD5^{R274W} does not express higher than wildtype ^{FLAGHA}OTUD5. hES H1 cells stably expressing doxycycline-inducible wildtype ^{FLAGHA}OTUD5 (WT), catalytically inactive ^{FLAGHA}OTUD5 (C224S), or patient variant ^{FLAGHA}OTUD5 (L352P, R274W) were induced with doxycycline (DOX) for 48h as indicated and subjected to anti-HA and anti-GAPDH immunoblot analysis.

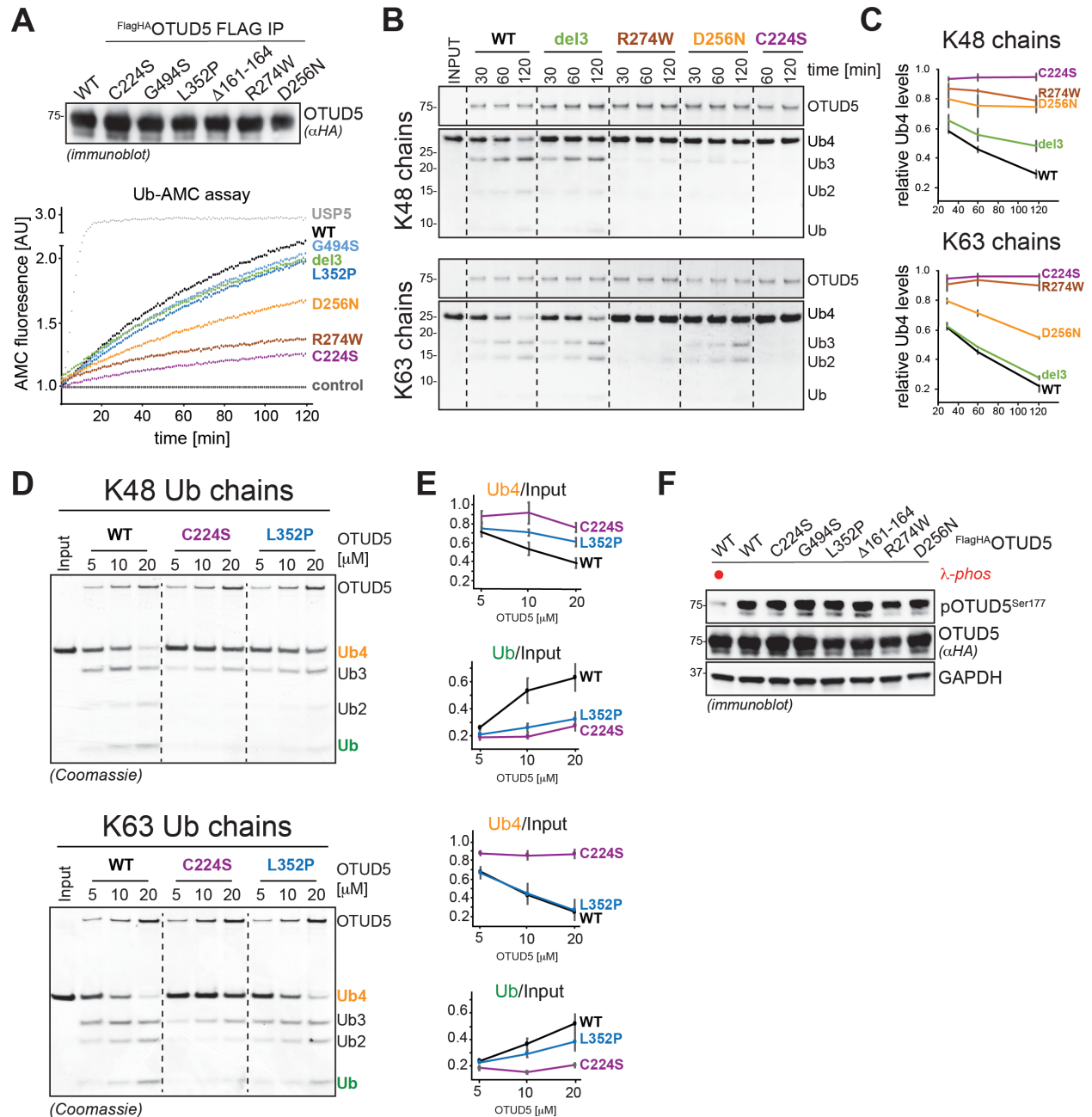


Fig. S3: Most patient mutations reduce OTUD5 deubiquitylation activity

A. The p.D256N and p.R274W mutations reduce OTUD5's ability to hydrolyze Ub-AMC, while other variants have no significant effect. *Upper panel:* Wildtype ^{FLAGHA}OTUD5 (WT), catalytically inactive ^{FLAGHA}OTUD5 (C224S), and denoted patient variant ^{FLAGHA}OTUD5 were purified from HEK293T cells followed by normalization and anti-HA immunoblotting. *Lower*

panel: Purified ^{FLAGHA}OTUD5 variants and ^{FLAGHA}USP5 were incubated with Ub-AMC and increase of AMC fluorescence was detected over time. Control = flag-IPs from HEK293T cells.

B. The p.D256N and p.R274W variants reduce OTUD5 cleavage activity towards K63- and K48-chains, while the p.161-164del variant specifically reduces K48-chain cleavage. HEK293T-purified wildtype ^{FLAGHA}OTUD5 (WT), catalytically inactive ^{FLAGHA}OTUD5 (C224S), and denoted patient variant ^{FLAGHA}OTUD5 were incubated with tetra-K48- or tetra-K63-chains for indicated time periods and analyzed by SDS PAGE. **C.** Quantification of three independent experiments shown in B (error bars denote s.e.m). Intensity of Ub4 band is relative to the sum of intensity of Ub3, Ub2, and Ub band. **D.** The p.L352P variant specifically reduces OTUD5's K48-chain cleavage activity. Increasing amounts of HEK293T-purified wildtype ^{FLAGHA}OTUD5 (WT), catalytically inactive ^{FLAGHA}OTUD5 (C224S), and patient variant ^{FLAGHA}OTUD5 (L352P) were incubated with K48- or K63-tetra-ubiquitin chains (Ub4) for 2h. Samples were analyzed by SDS PAGE. **E.** Quantification of three independent experiments shown in D (error bars denote s.e.m). Intensities of Ub4 or Ub bands are relative to intensity of Ub4 input band. **F.** Patient variants have no obvious impact on OTUD5's activating phosphorylation. Wildtype ^{FLAGHA}OTUD5 (WT), catalytically inactive ^{FLAGHA}OTUD5 (C224S), and denoted patient variant ^{FLAGHA}OTUD5 were expressed in HEK293T cells. Cells were lysed, treated with λ -phosphatase as indicated, and subjected to immunoblotting using indicated antibodies.

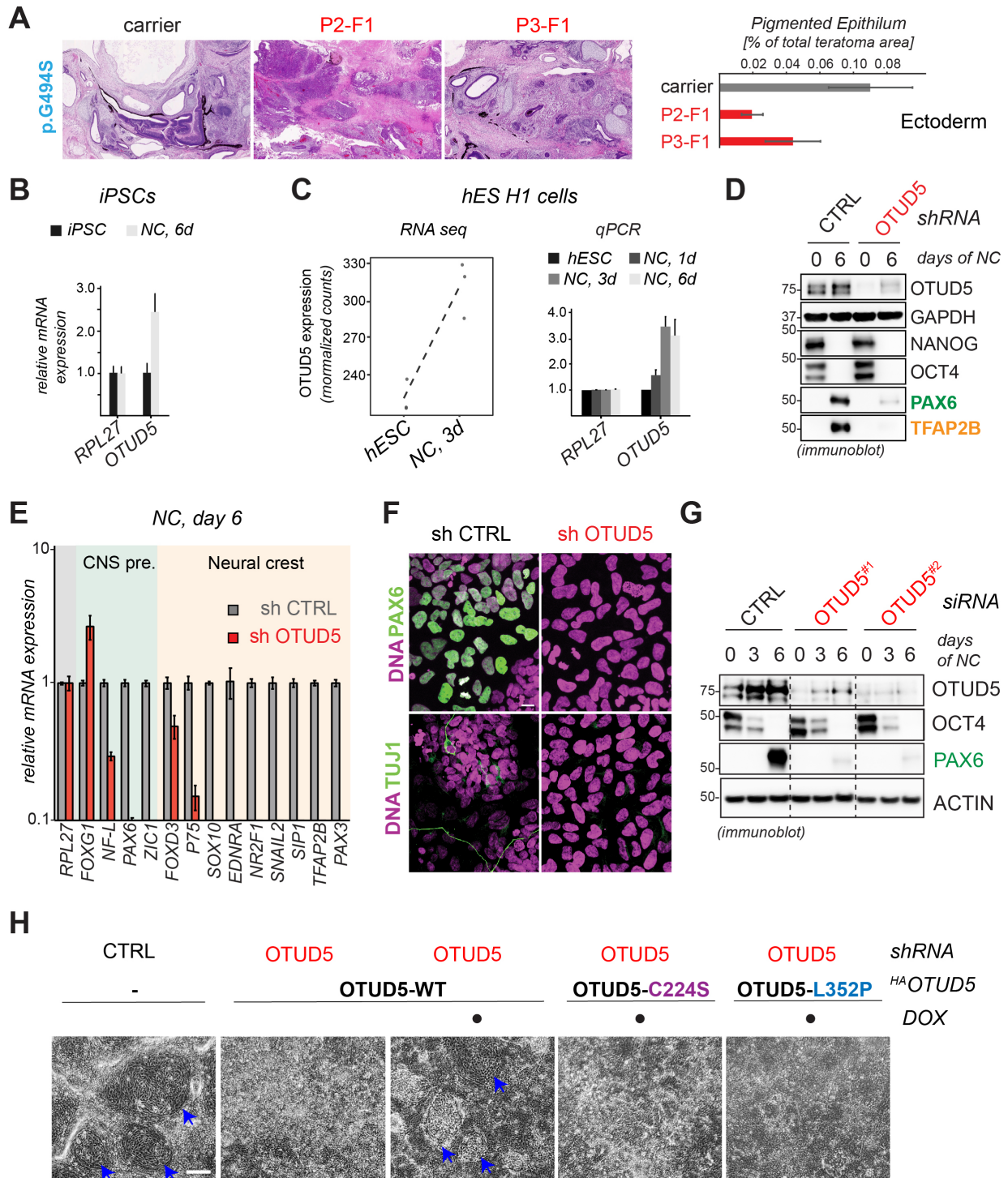


Fig. S4: Reduction of OTUD5 activity results in aberrant neuroectodermal differentiation

A. iPSCs derived from OTUD5 p.G494S patients are impaired in neuroectodermal differentiation *in vivo*, as evidenced by teratoma assays using p.Gly494Ser patient or maternal

control iPSCs. Teratoma sections were analyzed by H&E staining. Area occupied by pigmented epithelium (ectodermal marker) was quantified (error bars denote s.e.m, 12 slides of 2 teratomas per condition, * = $p < 0.05$, unpaired t-test). **B.** OTUD5 mRNA expression is upregulated during neural conversion of iPSCs, as evidenced by qRT-PCR. RPL27 = endogenous control (n=3 biological replicates, error bars denote s.d.). **C.** OTUD5 mRNA expression is upregulated during neural conversion of hESCs, as shown by RNA seq (left graph, n=3 biological replicates, FDR-adjusted q-value = 0.0004) or qRT-PCR (right graph, n=3 biological replicates, error bars denote s.d.) **D.** Depletion of OTUD5 from hESCs causes aberrant neural conversion, as monitored by immunoblotting using indicated antibodies. **E.** Depletion of OTUD5 from hESCs causes aberrant neural conversion, as evidenced by qRT-PCR for expression of CNS precursor markers (green) and neural crest markers (orange). RPL27 = endogenous control (n=3 technical replicates, error bars denote s.d.) **F.** Depletion of OTUD5 from hESCs causes aberrant neural conversion, as determined by immunofluorescence microscopy using antibodies against indicated neural markers. Scale Bar = 20 μ m. **G.** siRNA-mediated depletion of OTUD5 from hESCs cells causes aberrant neural conversion as shown by immunoblotting using indicated antibodies. **H.** K48-chain specific deubiquitylation activity of OTUD5 is required for neural conversion. Same experiment as in Figure 3E, but successful differentiation was determined by detection of neural rosette structures (blue arrows) using phase contrast microscopy.

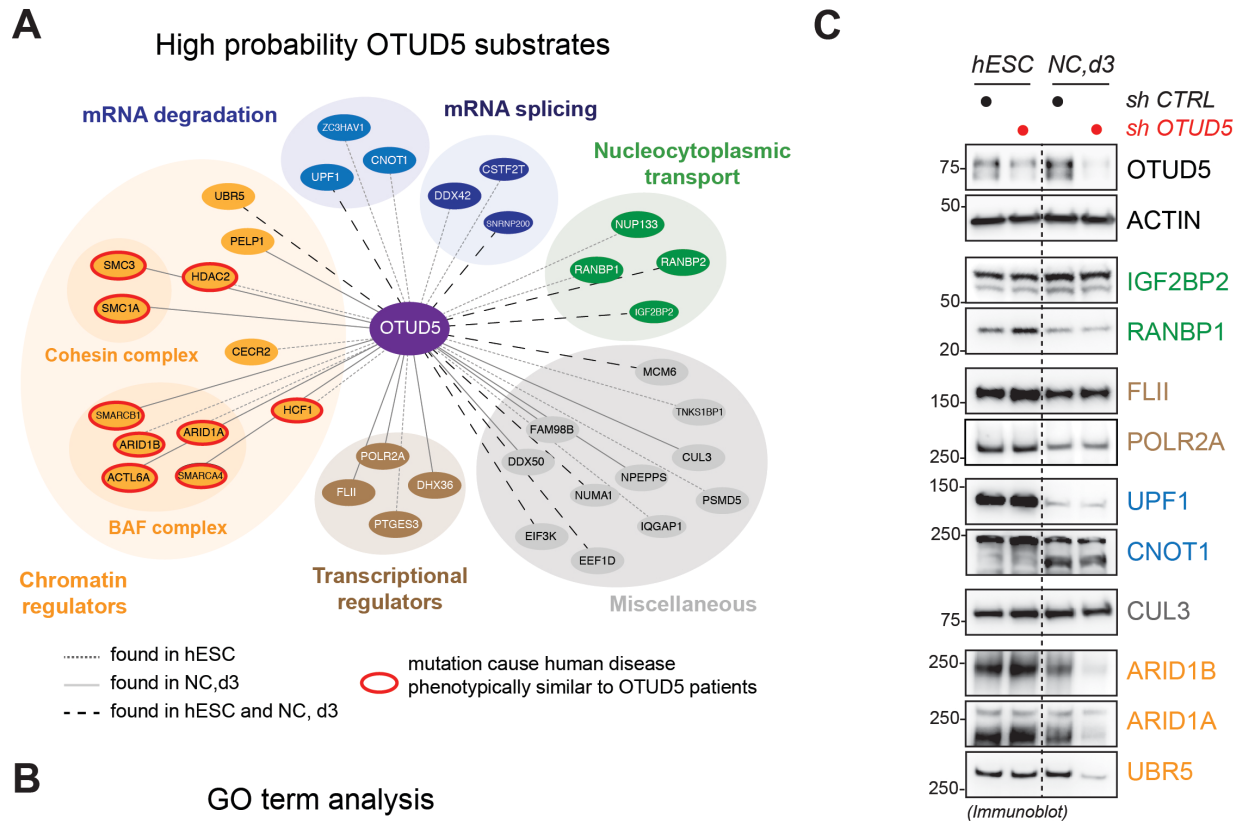


Fig. S5: OTUD5 interacts with chromatin regulators and regulates their stability specifically during differentiation

A. Schematic representation of high probability substrates of OTUD5. To identify high probability substrates of OTUD5 two independent proteomic experiments were performed (cf. Figure 3a). First, control or OTUD5-depleted H1 hESCs or hESCs undergoing neural conversion for 1 or 3 days were lysed and ubiquitylated proteins were isolated by TUBE pull down followed

by protein identification via mass spectrometry. Second, self-renewing or differentiating control hESCs or hESCs expressing wildtype (WT) or catalytically inactive (C224S)^{FLAG}OTUD5 were lysed and subjected to anti-FLAG immunoprecipitation followed by identification of interacting proteins via mass spectrometry. Candidate OTUD5 substrates were defined as proteins found to be more ubiquitinated upon OTUD5 depletion and identified as specific OTUD5 WT or C224S interactors. These high probability substrates of OTUD5 were functionally annotated and plotted using cytoscape. Color of lines indicate in which cell state the physical OTUD5 interaction occurred (dark grey: hES cell state (hESC), light grey: cells undergoing neural conversion for 3d (NC, d3), black: hESC and NC, d3). Candidate substrates that when mutated cause human diseases with phenotypic overlap to OTUD5 patients are circled in red. **B.** High probability substrates of OTUD5 are significantly enriched in chromatin regulators, as determined by GO term analysis. **C.** OTUD5 destabilizes chromatin remodelers, but not other tested candidate substrates identified by mass spectrometry in differentiating hESCs. Control or OTUD5-depleted hESCs or hESC subjected to neural conversion for 3 days were analyzed by immunoblotting with indicated antibodies.

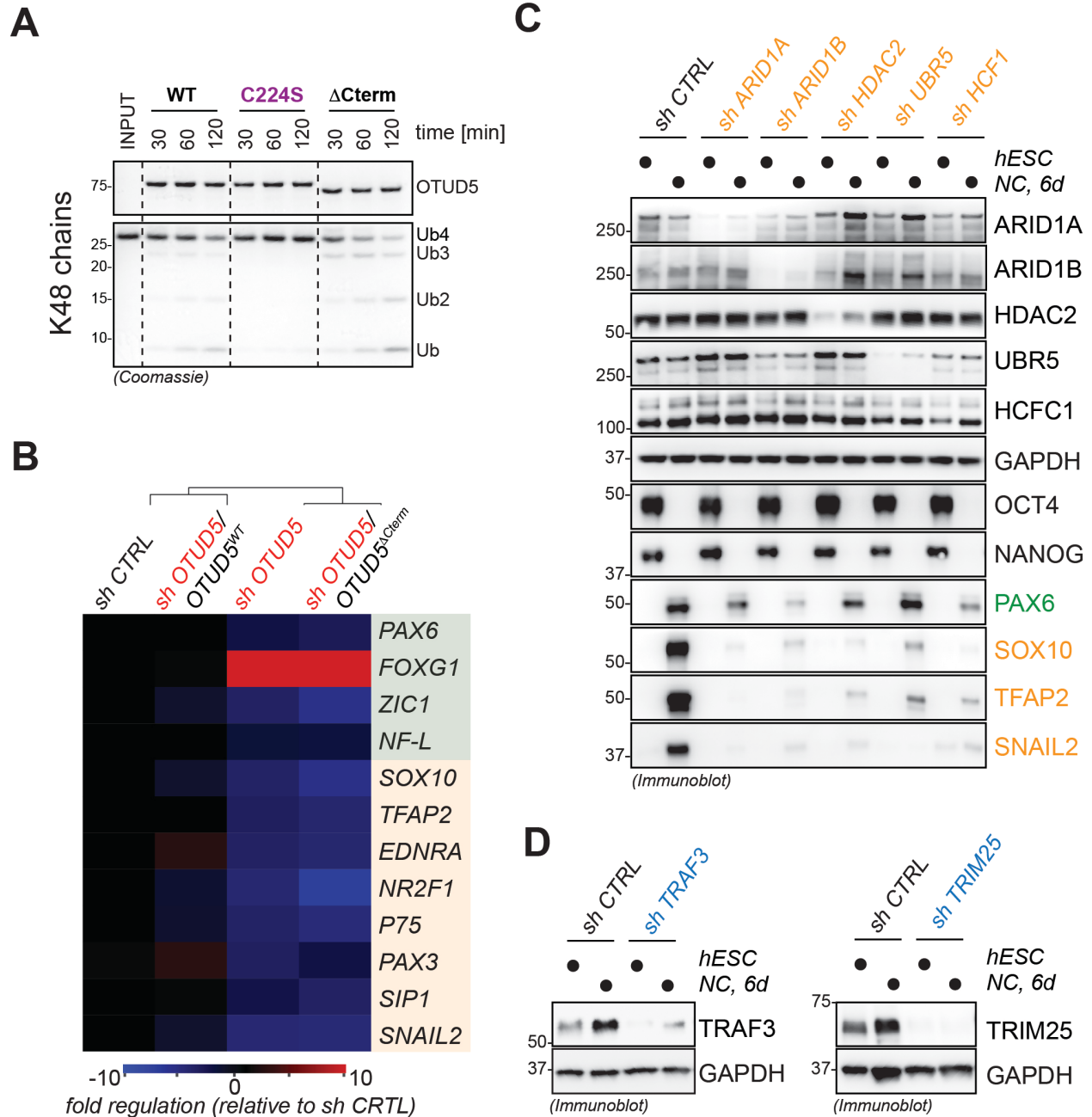


Fig. S6: OTUD5 regulates differentiation through stabilizing chromatin remodelers

A. Deletion of the C-terminus of OTUD5 containing the UIM motif does not reduce its K48-ubiquitin chain activity *in vitro*. Wildtype ^{FLAGHA}OTUD5 (WT), catalytically inactive ^{FLAGHA}OTUD5 (C224S), and chromatin regulator binding-deficient OTUD5 (Δ Cterm) were

purified from HEK293T cells and incubated with tetra-K48-chains for indicated time periods and

purified from HEK293T cells and incubated with tetra-K48-chains for indicated time periods and

analyzed by colloidal coomassie-stained SDS PAGE gels. **B.** The chromatin regulator binding-deficient $^{FLAGHA}OTUD5^{\Delta Cterm}$ mutant does not support neural conversion. hES H1 cells stably expressing shRNA-resistant and doxycycline-inducible wildtype (WT) or chromatin regulator binding-deficient ($\Delta Cterm$) $^{FLAGHA}OTUD5$. Cells were then depleted of endogenous OTUD5 using shRNA as indicated, treated with or without doxycycline (DOX), and subjected to neural conversion for 6 days. This was followed by qRT-PCR for expression of CNS precursor markers (highlighted in green) and neural crest markers (highlighted in orange). Marker expression was normalized to carrier control followed by hierarchical cluster analysis. RPL27 was used as endogenous control. **C.** Depletion of chromatin regulators results in aberrant neural conversion. hES H1 cells were depleted of endogenous indicated chromatin regulators using stably expressed shRNAs and subjected to neural conversion for 6 days and analyzed by immunoblotting to assess knockdown efficiency and the expression of CNS precursor marker (PAX6) and neural crest markers (SOX10, TFAP2, SNAIL2). GAPDH serves as loading control. **D.** Verification of knockdown of TRAF3 and TRIM25 in cells analyzed in the differentiation experiment shown in Figure 5E. hES H1 cells were depleted of endogenous TRAF3 and TRIM25 using stably expressed shRNAs, subjected to neural conversion for 6 days, and analyzed by immunoblotting.

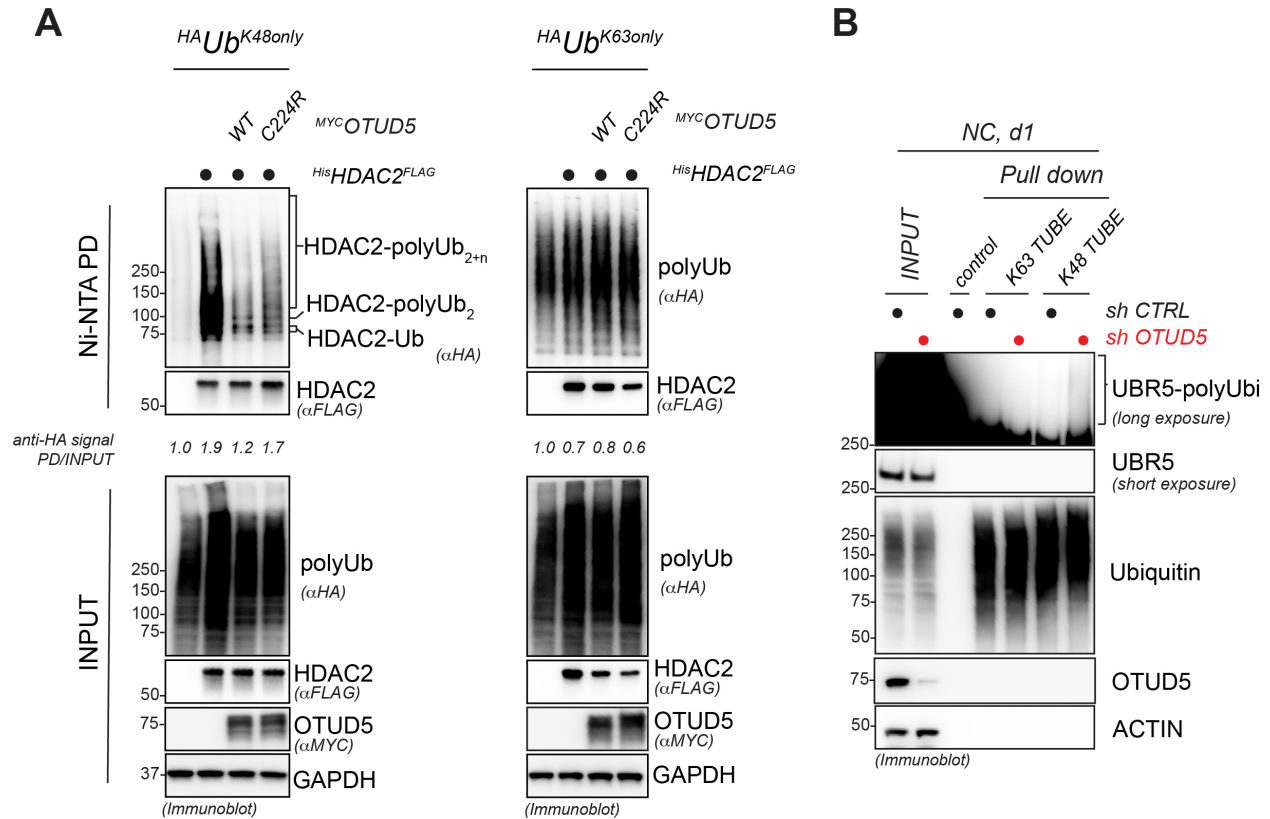


Fig. S7: OTUD5 cleaves K48-linked ubiquitin chains from chromatin remodeler substrates

A. HDAC2 is modified with K48-linked ubiquitin chains that can be shortened by wildtype (WT), but not catalytically inactive OTUD5 (C224R). HEK 293T cells were transfected with *His*HDAC2 and HA-tagged ubiquitin variants that only allow for formation of K48-linked chains (*HA Ub^{K48only}*, left panel) or formation of K63-linked chains (*HA Ub^{K63only}*, right panel) in the absence or presence of MYC-tagged, wildtype or catalytically inactive OTUD5 (*MYC OTUD5^{WT}* or *C224R*). Cells were treated with MG132 for 4h, lysed, and subjected to denaturing NiNTA pull down (PD) followed by immunoblotting with indicated antibodies. In these assays, a specific portion of *His*HDAC2 is modified by K48-linked ubiquitin chains, as evidenced by a ~2-fold increase in the anti-HA signal NiNTA PD/INPUT ratio in the *His*HDAC2 condition over the control, which was set to 1 (left panel, lane 2 vs. 1). These K48-linked ubiquitin chains on *His*HDAC2 can be reduced and trimmed by wild type OTUD5, but less by catalytically inactive

OTUD5^{C224R}. Of note, there is higher expression of HAUb^{K48only} when co-transfected with HisHDAC2 in the absence of MYCOTUD5^{WT} or ^{C224R}. Under these experimental conditions, HisHDAC2 is not specifically modified by K63-linked ubiquitin chains (right panel) **B**. OTUD5 depletion in hES cells undergoing early stages of neural conversion results in an increase in endogenous UBR5 that is modified with K48-linked, but not with K63-linked ubiquitin chains. hES H1 cells were depleted of endogenous OTUD5 using stably expressed shRNAs, subjected to neural conversion for 1 day, treated with proteasome inhibitor for 4h, ubiquitylated proteins were isolated by pull down with K48- or K63-ubiquitin-chain specific TUBES, and samples were analyzed by immunoblotting with indicated antibodies. Empty beads were used as pull down control.

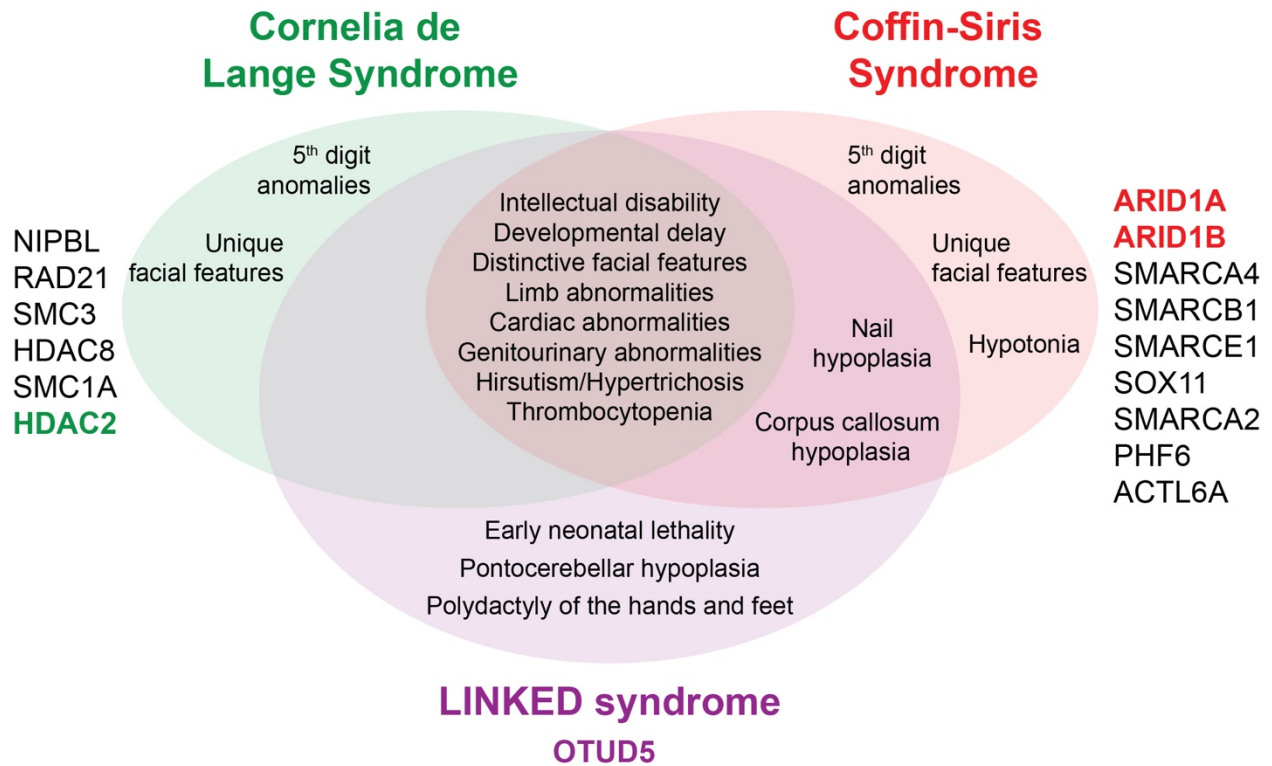


Fig. S8: Venn Diagram depicting the unique and overlapping features of LINKED patients and patients suffering from Cornelia de Lange and Coffin-Siris Syndrome

Genes whose mutations cause the respective diseases are depicted. HDAC2 and ARID1A/B, substrates of OTUD5, are highlighted in bold.

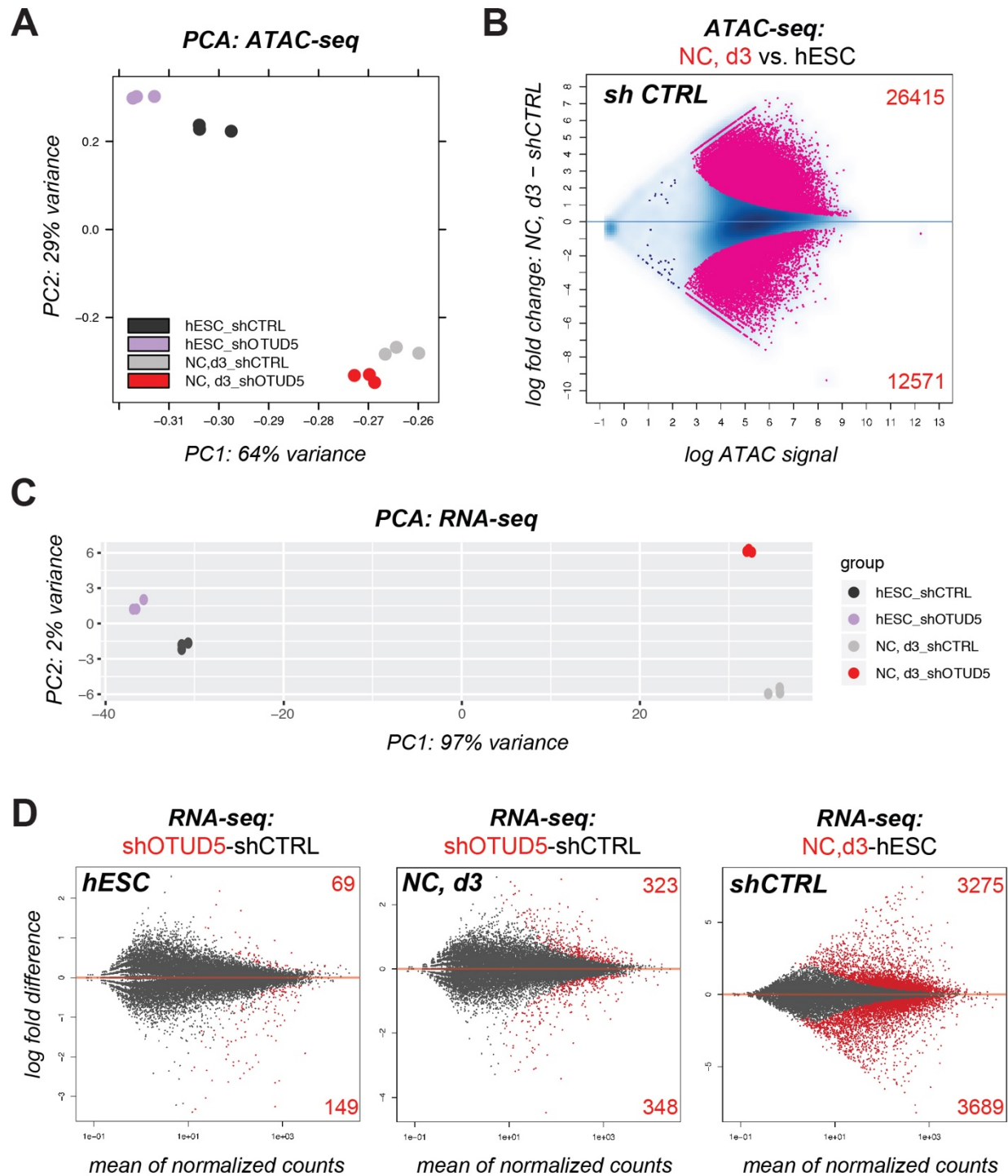


Fig. S9: Chromatin accessibility and transcriptome remain largely unchanged upon loss of OTUD5 during early differentiation

A. Principal component analysis (PCA) of chromatin accessibility (assayed by ATAC-seq) of control and OTUD5-depleted hES H1 cells (hESC) and cells subjected to neural conversion for three days (NC, d3). OTUD5 has only minor effects on the overall chromatin landscape as compared to the differences observed during neural conversion (hESC versus NC3,d). **B.** MA-plot highlighting the drastically different ATAC-seq profiles between self-renewing hES H1 cells (hESC) and cells undergoing neural conversion for 3 days (NC, d3). Peaks represented in the top part of the plot gain accessibility during differentiation while peaks in the bottom half, lose accessibility. Pink dots represent peaks with statistically significant enrichment differences (adj pvalue < 0.0001) between the two conditions. Note that these changes are drastically more different than differences observed comparing control and OTUD5-depleted cells at NC, d3 in Figure 4a, suggesting that OTUD5-dependent chromatin accessibility changes are not a mere consequence of failed differentiation. **C.** PCA of transcriptional profiles, assayed using RNAseq, in control and OTUD5-depleted hESC and cells subjected to neural conversion for 3 days (NC, d3). OTUD5 depletion has little effect on transcriptional state of hESCs as compared to the difference in profiles evident at NC, d3 stage. 97% of the transcriptional variance is related to differentiation. **D.** MA-plots illustrating the minimal impact of OTUD5 loss on transcription in hESCs (left panel), which is slightly increased at day 3 of neural conversion (NC, d3, middle panel). OTUD5-dependent transcriptional changes at hESC (left panel), and NC, d3 (center panel) are modest compared to transcriptional alterations during differentiation in control cells (right panel).

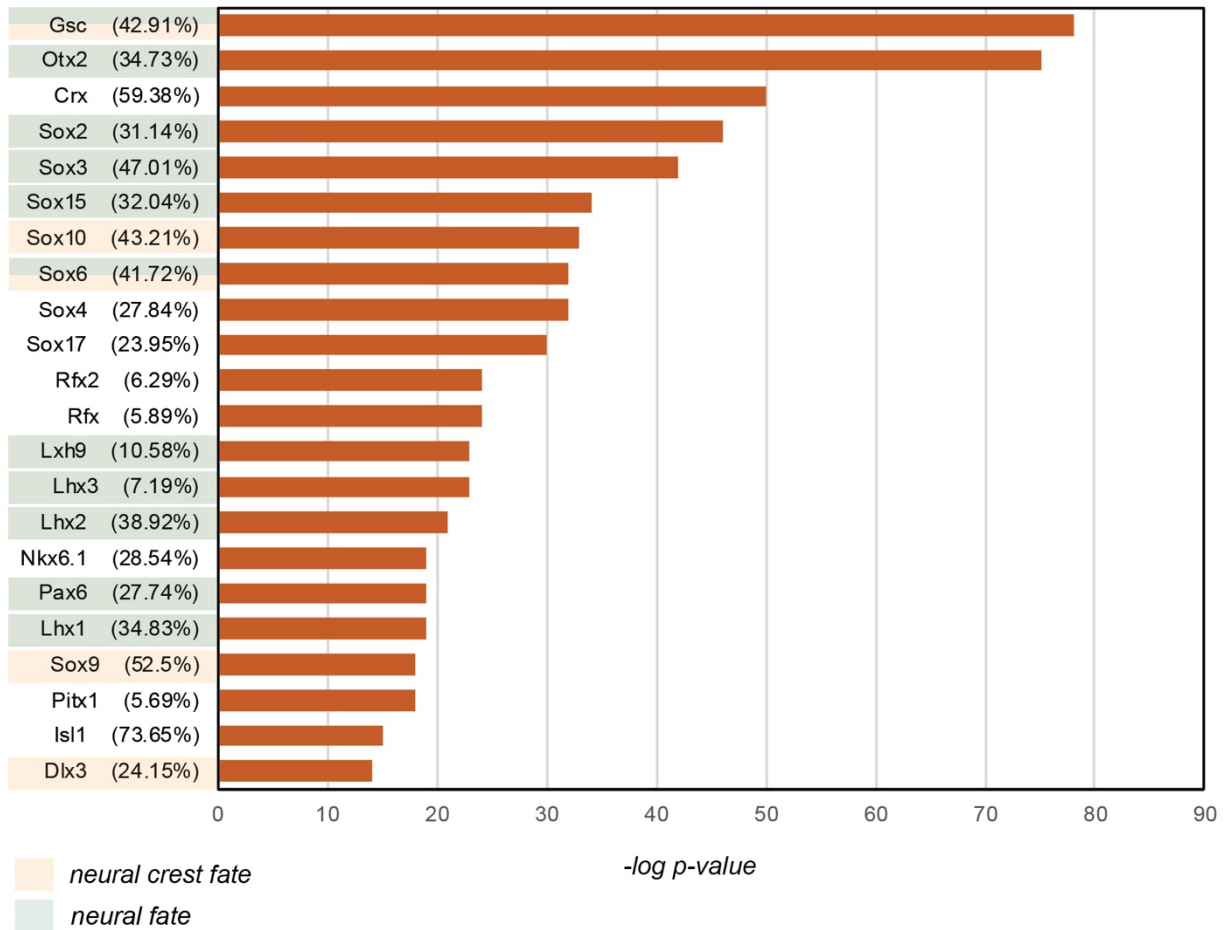


Fig. S10: OTUD5-regulated enhancers are enriched in motifs for neural- and neural-crest promoting transcription factors

Transcription factor motif analysis was performed on the ATAC-seq regions that were labeled as potential enhancers and that lost chromatin accessibility upon OTUD5 loss at day 3 of neural conversion. These regions are enriched for transcription factors important for driving differentiation towards a neural fate (highlighted in green) or neural crest fate (highlighted in orange). Numbers in parenthesis represent the fraction of enhancers that contain the respective transcription factor motifs.

Table S1: Detailed clinical information on OTUD5-deficient patients

Table S2: Proteins differentially binding to TUBE_s upon OTUD5 depletion.

Table S3: Proteins physically interacting with OTUD5 in self renewing and differentiating hESCs.

Table S4: High probability targets of OTUD5.

Table S5: qRT-PCR primers used in this study

List of members of the Undiagnosed Diseases Network (alphabetical order):

Maria T. Acosta, Margaret Adam, David R. Adams, Pankaj B. Agrawal, Mercedes E. Alejandro, Patrick Allard, Justin Alvey, Laura Amendola, Ashley Andrews, Euan A. Ashley, Mahshid S. Azamian, Carlos A. Bacino, Guney Bademci, Eva Baker, Ashok Balasubramanyam, Dustin Baldrige, Jim Bale, Michael Bamshad, Deborah Barbouth, Gabriel F. Batzli, Pinar Bayrak-Toydemir, Anita Beck, Alan H. Beggs, Gill Bejerano, Hugo J. Bellen, Jimmy Bennet, Beverly Berg-Rood, Raphael Bernier, Jonathan A. Bernstein, Gerard T. Berry, Anna Bican, Stephanie Bivona, Elizabeth Blue, John Bohnsack, Carsten Bonnenmann, Devon Bonner, Lorenzo Botto, Lauren C. Briere, Elly Brokamp, Elizabeth A. Burke, Lindsay C. Burrage, Manish J. Butte, Peter Byers, John Carey, Olveen Carrasquillo, Ta Chen Peter Chang, Sirisak Chanprasert, Hsiao-Tuan Chao, Gary D. Clark, Terra R. Coakley, Laurel A. Cobban, Joy D. Cogan, F. Sessions Cole, Heather A. Colley, Cynthia M. Cooper, Heidi Cope, William J. Craigen, Michael Cunningham, Precilla D'Souza, Hongzheng Dai, Surendra Dasari, Mariska Davids, Jyoti G. Dayal, Esteban C. Dell'Angelica, Shweta U. Dhar, Katrina Dipple, Daniel Doherty, Naghmeh Dorrani, Emilie D. Douine, David D. Draper, Laura Duncan, Dawn Earl, David J. Eckstein, Lisa T. Emrick, Christine M. Eng, Cecilia Esteves, Tyra Estwick, Liliana Fernandez, Carlos Ferreira, Elizabeth

L. Fieg, Paul G. Fisher, Brent L. Fogel, Irman Forghani, Laure Fresard, William A. Gahl, Ian Glass, Rena A. Godfrey, Katie GoldenGrant, Alica M. Goldman, David B. Goldstein, Alana Grajewski, Catherine A. Groden, Andrea L. Gropman, Sihoun Hahn, Rizwan Hamid, Neil A. Hanchard, Nichole Hayes, Frances High, Anne Hing, Fuki M. Hisama, Ingrid A. Holm, Jason Hom, Martha Horike-Pyne, Alden Huang, Yong Huang, Rosario Isasi, Fariha Jamal, Gail P. Jarvik, Jeffrey Jarvik, Suman Jayadev, Yong-hui Jiang, Jean M. Johnston, Lefkothea Karaviti, Emily G. Kelley, Dana Kiley, Isaac S. Kohane, Jennefer N. Kohler, Deborah Krakow, Donna M. Krasnewich, Susan Korrick, Mary Koziura, Joel B. Krier, Seema R. Lalani, Byron Lam, Christina Lam, Brendan C. Lanpher, Ian R. Lanza, C. Christopher Lau, Kimberly LeBlanc, Brendan H. Lee, Hane Lee, Roy Levitt, Richard A. Lewis, Sharyn A. Lincoln, Pengfei Liu, Xue Zhong Liu, Nicola Longo, Sandra K. Loo, Joseph Loscalzo, Richard L. Maas, Ellen F. Macnamara, Calum A. MacRae, Valerie V. Maduro, Marta M. Majcherska, May Christine V. Malicdan, Laura A. Mamounas, Teri A. Manolio, Rong Mao, Kenneth Maravilla, Thomas C. Markello, Ronit Marom, Gabor Marth, Beth A. Martin, Martin G. Martin, Julian A. Martínez-Agosto, Shruti Marwaha, Jacob McCauley, Allyn McConkie-Rosell, Colleen E. McCormack, Alexa T. McCray, Heather Mefford, J. Lawrence Merritt, Matthew Might, Ghayda Mirzaa, Eva Morava-Kozicz, Paolo M. Moretti, Marie Morimoto, John J. Mulvihill, David R. Murdock, Avi Nath, Stan F. Nelson, John H. Newman, Sarah K. Nicholas, Deborah Nickerson, Donna Novacic, Devin Oglesbee, James P. Orengo, Laura Pace, Stephen Pak, J. Carl Pallais, Christina GS. Palmer, Jeanette C. Papp, Neil H. Parker, John A. Phillips III, Jennifer E. Posey, John H. Postlethwait, Lorraine Potocki, Barbara N. Pusey, Aaron Quinlan, Wendy Raskind, Archana N. Raja, Genecee Renteria, Chloe M. Reuter, Lynette Rives, Amy K. Robertson, Lance H. Rodan, Jill A. Rosenfeld, Robb K. Rowley, Maura Ruzhnikov, Ralph Sacco, Jacinda B. Sampson, Susan

L. Samson, Mario Saporta, C. Ron Scott, Judy Schaechter, Timothy Schedl, Kelly Schoch, Daryl A. Scott, Lisa Shakachite, Prashant Sharma, Vandana Shashi, Jimann Shin, Rebecca Signer, Catherine H. Sillari, Edwin K. Silverman, Janet S. Sinsheimer, Kathy Sisco, Kevin S. Smith, Lilianna Solnica-Krezel, Rebecca C. Spillmann, Joan M. Stoler, Nicholas Stong, Jennifer A. Sullivan, Angela Sun, Shirley Sutton, David A. Sweetser, Virginia Sybert, Holly K. Tabor, Cecelia P. Tamburro, Queenie K.-G. Tan, Mustafa Tekin, Fred Telischi, Willa Thorson, Cynthia J. Tifft, Camilo Toro, Alyssa A. Tran, Tiina K. Urv, Matt Velinder, Dave Viskochil, Tiphonie P. Vogel, Colleen E. Wahl, Stephanie Wallace, Nicole M. Walley, Chris A. Walsh, Melissa Walker, Jennifer Wambach, Jijun Wan, Lee-kai Wang, Michael F. Wangler, Patricia A. Ward, Daniel Wegner, Mark Wener, Monte Westerfield, Matthew T. Wheeler, Anastasia L. Wise, Lynne A. Wolfe, Jeremy D. Woods, Shinya Yamamoto, John Yang, Amanda J. Yoon, Guoyun Yu, Diane B. Zastrow, Chunli Zhao, Stephan Zuchner.